



Optics Letters

Resolution enhanced photothermal imaging by high-order correlation

XIAOBING SUNIAN,¹  WEI LIU,² LEI CHEN,² ZHIHAO ZHOU,¹ DONGYI SHEN,²  YUEHAN LIU,³ AND WENJIE WAN^{1,2,*} 

¹MOE Key Laboratory for Laser Plasmas and Collaborative Innovation Center of IFSA, The University of Michigan-Shanghai Jiao Tong University Joint Institute, Shanghai Jiao Tong University, Shanghai 200240, China

²The State Key Laboratory of Advanced Optical Communication Systems and Networks, Department of Physics and Astronomy, Shanghai Jiao Tong University, Shanghai 200240, China

³Whiting School of Engineering, Johns Hopkins University, Baltimore, Maryland 21218, USA

*Corresponding author: wenjie.wan@sjtu.edu.cn

Received 4 May 2020; revised 17 September 2020; accepted 21 September 2020; posted 21 September 2020 (Doc. ID 396780); published 9 October 2020

Laser scanning photothermal imaging offers a powerful non-destructive testing tool to visualize subsurface structures of opaque materials, but it suffers the resolution limit imposed by thermal diffusion. To overcome this physical obstacle, a tightly focused excitation beam with a high repetition rate is usually used to improve the spatial resolution. Here, we demonstrate that the resolution of photothermal imaging could be enhanced using the high-order correlation imaging method inspired by correlated optical imaging. By carefully designing the laser scanning and modulation behavior, we can individually control the statistical properties of isolated hotspots induced by lasers. Imaging reconstructions of subsurface structures are performed afterward by reading out time-fluctuated thermal images. Moreover, the resolution can be further enhanced by using the high-order correlation, which enables a new way for highly resolved thermal imaging and metrology applications. © 2020 Optical Society of America

<https://doi.org/10.1364/OL.396780>

Photothermal imaging (PTI) capable of characterizing the sample surface temperature enables a unique solution for non-destructive testing of the subsurface structure of opaque material with the help of laser scanning infrared (IR) thermography [1–3]. Subsurface imaging offers an accurate tool to visualize the subsurface structures, such as defects of crack, scratch, and thermal inhomogeneity within materials [4,5]. Conventionally, the pump–probe configuration is based on laser scanning for both excitation and detection of the modulated thermal signals [6]. The resolution of PTI, the ability to distinguish two nearby objects with a distinguishable contrast, depends on the sizes of the pump and probe beams, the excitation and detection schemes of thermal waves, the thermal properties of the material, the geometry of the targets, and the chopping frequency of the pump beam [7–9]. No matter whether it is detecting subsurface defects directly, the resolution of PTI can be improved by combining optical methods or processing with higher focusing and higher repetition rates of the beams [10–15].

On the other hand, the temporally varying intensities of thermal signals provide us an opportunity to improve the image resolution by employing the intensity correlation imaging method, which is better known as the super-resolution optical fluctuation imaging (SOFI) method [16]. SOFI is one of the super-resolution fluorescence microscopy techniques that can break the diffraction limit of light and improve imaging resolution. Differing from other techniques such as stimulated emission depletion microscopy (STED) [17] or structured illumination microscopy (SIM) [18] based on patterned illumination, SOFI relies on exploring statistical properties of light, much like photo-activation localization microscopy (PALM) [19] and stochastic optical reconstruction microscopy (STORM) [20]. Later, modified versions of SOFI [21–23] have also been proposed to improve the image quality further. Among these modified schemes, the high-order correlation imaging method based on analyzing the statistical properties of blinking optical emitters can offer another alternative to address some issues in conventional correlation imaging such as computation time and brightness distortion [24]. If combined with thermal emitters, such correlation imaging methods are expected to enhance the resolution of PTI, enabling highly resolved PTI.

In this Letter, we experimentally demonstrate the proof of concept results where resolution enhanced PTI is achieved based on high-order correlation reconstruction. In this work, an IR camera is used to capture the radiated IR light to measure the temperature directly. By tracing temporally varying IR signals of each pixel and computing their corresponding high-order correlations, this method provides a means to localize thermal emitters against its thermal background, where material thermal diffusion dominates during the thermal emitting process. Theoretically, the resolution depends on the pixel size, repetition rate, and size of the excitation beam. Temporal correlations of thermal signals with different orders are computed to show that the enhancement factor for resolution can be significantly improved with increasing order and finally can reach the sub-wavelength of the resolution. Moreover, a subsurface structure imaging can be formed with improved resolution using the

current method, although it is not visible through traditional optical imaging. Compared to the conventional non-destructive detection technique of using ultrasound or photoacoustic elastography, this technique can achieve far-field detection, multi-pixel imaging, and ultrasound-protective imaging. This technique opens up a new avenue for thermal imaging in biomedical and metrology areas.

Figure 1(a) shows the schematic of the PTI process: a temporally modulated laser is tightly focused onto a double-layer sample, which consists of a strong-absorbing top layer with a thickness of z_0 and a metal substrate. Once the top surface absorbs the laser, localized heat is excited and then diffuses away, forming a localized thermal emitter. The conduction of the diffusive heat is heavily damped through thermal waves, which subsequently interact with the microstructures at the coating/substrate interface, which can modify the surface temperature distribution $T(x, y, 0)$. As a result, $T(x, y, 0)$ can depict the subsurface structure even if it is embedded under the sample at the position (x, y, z_0) . This offers PTI a unique capability of seeing below surfaces. Mathematically, $T(x, y, 0)$ can be obtained by solving the heat diffusion equation with spatially dependent coefficients performing a perturbation theoretical approach [11].

We consider a point-like subsurface thermal target. $T(x, y, 0)$ accordingly consists of a nonzero background mean term T_0 and a deviation term T_{dev} . The latter term depends on the deviation of the thermal conductivity $\kappa(r)$ of the point-like target from that of the surrounding medium. In this case, T_{dev}/T_0 is identical to the thermal point spread function of PTI that is called $G(r)$. When evaluating the quality of PTI, it is convenient to use the formalism of this function, which describes the blurring of the image of a point object as the result of the physical mechanism of image formation [9]. With the laser modulation frequency taking the value of ω , $G(r)$ is given as

$$G(r) \propto \exp\left[-\frac{1+i}{\mu}\left(z_0 + \sqrt{r^2 + z_0^2}\right)\right], \quad (1)$$

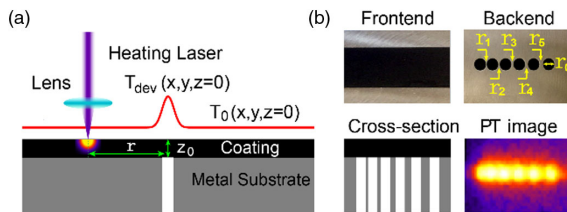


Fig. 1. (a) Scheme of PTI of a subsurface air hole of a double-layer sample using point-like heating and a large area detector. The double-layer sample consists of a strongly absorbing opaque coating layer of thickness z_0 and a metal substrate. Scanning the laser focus can localize the subsurface structure against the homogeneous thermal background (T_0) in the form of a thermal deviation (T_{dev}), which visualizes the inside of the sample. (b) Resolution limited PTI of subsurface air holes in the opaque double-layer sample. The sample is constructed by bonding an opaque tape on a metal plate (304 stainless steel). Six air holes with a radius of $r_0 = 0.5$ mm are dug on the metal substrate. The pitches of the air holes are $r_1 = 0.4$ mm, $r_2 = 0.6$ mm, $r_3 = 0.8$ mm, $r_4 = 1.0$ mm, and $r_5 = 1.2$ mm. 2D scanning of the laser over the front surface of the sample can produce the differentiable photothermal image of the air holes from the surrounding medium, but the air holes cannot be resolved from each other because of the thermal diffusion.

where $\mu = \sqrt{2\kappa/\omega\rho c}$ is the thermal diffusion length with (ρc) being the heat capacity per unit volume. The thermal diffusion length describes the distance over which the thermal wave decreases to its $1/e$ value. $G(r)$ implies that the image of a point-like thermal object extends to a blurring hotspot because of the heat diffusion so that the resolution of PTI is limited, which is analogous to the diffraction limit of optical imaging.

Generally, the resolution of the laser-scanning PTI can be quantified in terms of half-width at half-contrast function (HWHC) [11]. Since the amplitude contrast function mathematically equals $\text{Re}(G)$, the resolution is thus connected with $G(r)$. We further consider the Gaussian-distributed laser beam $F(r)$ with the diameter of $2R$ and the extended thermal target. G can be replaced by using an extended thermal point spread function $U(r)$ [24]. By this consideration, the minimum distinguishable lateral distance D_0 between two close-by thermal targets equals $2\sqrt{R^2 + \mu^2}$, which indicates that the resolution of the laser-scanning PTI depends on the focus size and thermal diffusion length. As Fig. 1(b) shows, the thermal targets are indistinguishable in the directly obtained image because the maximum pitch of the air holes dug on the metal substrate is smaller than the resolution limit D_0 .

In order to improve image resolution, the width of $U(r)$ must be reduced. Here, we utilize the high-order correlation imaging method that analyzes the statistical temporal properties of the fluctuating thermal emitters: taking a movie of numerous images instead of a single shot image to compute the temporal correlations. To get this method applied to the laser-scanning PTI, we assume that the sample surface just above the thermal target is labeled with N single thermal emitters. Under this assumption, the intensity fluctuation of the thermal emitters can be accomplished by adjusting the scanning and modulation behavior of the laser beam. Specifically, thermal emitters turn on once illuminated by the laser but turn off after the heat diffuses away.

Combined with the thermal emitter model, the thermal signal at space-time position (r, t) is given by the convolution of the thermal emitter distribution $T(r, t)$ and the system's thermal point spread function $U(r)$. Inspired by the optical high-order correlation imaging (HG) method [12], the n th-order correlation function $\text{HG}_n(r, \tau_1, \dots, \tau_{n-1})$ is thus expressed as

$$\text{HG}_n(r, \tau_1, \dots, \tau_{n-1}) = \sum_k U^n(r - r_k) \langle |\delta T(r_k, t) \cdot \delta T(r_k, t + \tau_0) \cdots \delta T(r_k, t + \tau_{n-1})| \rangle, \quad (2)$$

with $(\tau_{01} = \tau_1 - \tau_0, \dots, \tau_{0n-1} = \tau_{n-1} - \tau_0)$, where $\tau_{j=0, \dots, n-1}$ is time lag between two movie frames, and $\langle \dots \rangle_t$ denotes time averaging. It should be noted that the n th-order correlation image given by HG_n is not presented by the thermal emitter intensity but by the convolution of a new thermal point spread function $U' = U^n(r - r_k)$ and the degree of n th-order correlation of the emitter intensity [16].

Inspired by the recent work, which shows that the resolution and contrast of the third-order ghost imaging depend on the “directionality” of the spatial third-order correlation function, we choose the proper time lags to reduce the huge memory and the complicated computation [25]. Consequently, while in the case of $\tau_{01} + \tau_{02} + \dots + \tau_{0n-1} = 0$, the width of the n

th-order temporal correlation function tends to be narrower. It is further concluded that the greater the variables differ from each other, the narrower the width of the correlation function will be [24]. Under this condition, “time lags” of the fourth- and ninth-order correlations can be set as $(-2\tau, -\tau, \tau, 2\tau)$ and $(-4\tau, -3\tau, -2\tau, -\tau, \tau, 2\tau, 3\tau, 4\tau)$, for example. From Eq. (2), the width of the new thermal point spread function U' is reduced by a factor of \sqrt{n} compared to the original one, which leads to the \sqrt{n} -fold of resolution enhancement for HG_n imaging.

Experimentally, the setup of the laser-scanning PTI is illustrated in Fig. 2(a). It consists of a laser source (473 nm, 500 mw), an optical chopper, two mirrors, a scan lens (Thorlabs FTH254-1064), an IR camera (Seek Compact Pro), and a double-layer testing sample. The double-layer sample is constructed by bonding a commonly used opaque tape on the metal substrate (stainless steel 304) with air structures designed on the substrate. The thickness of the tape and the metal plate are $l_c = 0.143$ mm and $l_s = 1$ mm, respectively. The laser beam, which is focused on the sample with a radius of $R = 0.35$ mm, is modulated by a chopper. A series of step-like laser pulses with varying durations and intervals are accordingly produced. The low repetition rate $f_m \sim 1$ Hz \pm 0.1 Hz of the laser pulses ensures that the signal for the metal layer can respond to the disturbance of the laser modulation, while the signal for the air layer cannot. Two mirrors are bonded on the DC step motors, one of which rotates horizontally while the other one rotates vertically, accomplishing the scanning of the laser all over the sample surface. Here, the focused laser spot scans the surface plane with a frequency f_s of 0.3 Hz \pm 0.1 Hz. Besides, a scan lens ensures the uniform size of the laser focus and is beneficial for some special applications where the measuring object is required to be stationary. Meanwhile, the surface temperature oscillations are collected by the IR camera with the frame rate of $f_i = 15$ Hz.

Under these conditions, temporally fluctuating thermal signals radiated from the surface above the metal substrate

(blue line) and intensities of the thermal emitters (red line) produced at the surface just above the thermal target are illustrated as Fig. 2(b). The degree of second-order correlations of these thermal signal-intensity fluctuations is a function of time lag τ , as shown in Fig. 2(c), which shows that the second-order correlation of thermal emitters has a higher value than that of the thermal signals produced at the surroundings. Specifically, surface temperature above both the air region and the metal region rapidly grow and attempt to keep steady once illuminated by the laser but fall into the ambient temperature if the laser focus moves away. However, the latter decreases faster than the former one because the metal has a higher thermal conductivity.

Consequently, as shown in Fig. 2(b), the surface temperature modulation above the metal substrate is more sensitive to the laser modulation than the one above the air, resulting in slightly quicker temperature oscillations above the metal. As a result, even under the same laser excitation, surface temperature fluctuation induced above the metal (T_{Metal}) contains higher frequency components, while the air structure (T_{Air}) oscillates in a slower pace, exhibiting a higher second-order correlation of T_{Air} (red curve) in the low time-lag regime in Fig. 2(c), which helps us distinguish thermal emitters from the background thermal noise. Consequently, unlike using the lock-in technique in traditional PTI, the application of the HG method to the laser-scanning PTI provides us a new way that can locate the position of the thermal target and meanwhile enhance the contrast to the imaging.

For PTI imaging, the values of $HG_n(r, \tau_1, \dots, \tau_{n-1})$ of each pixel in our thermal camera are calculated to reconstruct correlation images [12]. As shown in Eq. (2), it appears as a sum of the new thermal point spread function. The physical meaning of HG_n is the correlation of the thermal signals from a single thermal emitter in one pixel. The thermal signals are detected at different times with the time lags of $(\tau_1, \dots, \tau_{n-1})$. Taking the specially designed time lags as previously mentioned, the width of the new thermal point spread function is reduced by a factor of \sqrt{n} , directly increasing the resolution by \sqrt{n} . In addition, the factor of the resolution enhancement is expected to increase with the orders increasing. As a result, since the resolution limit of the mean image is $D_0 \approx 2.21$ mm, the resolution of the HG_{25} image is $D_0/5 \approx 0.442$ mm. In order to verify the aforementioned concept of high-order correlation imaging and explore the factor of the corresponding resolution enhancement, we experimentally generate correlation images of different orders of an isolated thermal emitter. As shown in Fig. 3, images of an isolated thermal emitter are obtained based on the correlation method. By the cross section of the isolated thermal emitter plotted in Fig. 3(b), the width of the curve in the mean image with a width of about 2.25 mm shrinks to be sharper and sharper with the correlation orders increasing, resulting in the width of the curves of the 2nd-, 4th-, 9th-, 16th-, and 25th-order HG images being reduced to 1.33 mm, 1.23 mm, 0.99 mm, 0.72 mm, and 0.60 mm. As is revealed in Fig. 3(c), the experimental value fits well with the theoretical \sqrt{n} -fold resolution improvement of the simulation within an acceptable experimental error.

We further design a two-dimensional (2D) sample with six grooves on the metal substrate, shown as Fig. 4(a). Here, the air grooves serve as the thermal targets. The modulation and scanning behaviors of the laser are set as previously mentioned. The surface tape layer of the sample is opaque so that people

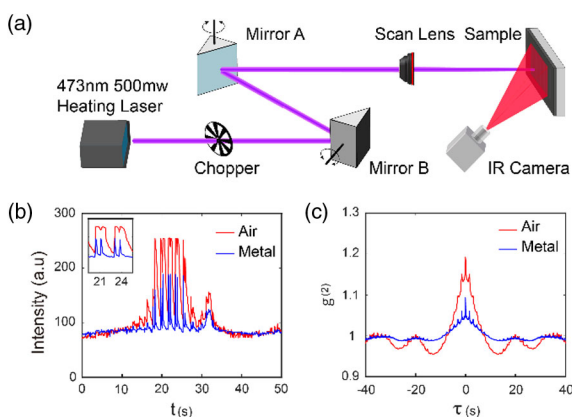


Fig. 2. (a) Experimental setup of the laser-scanning PTI. (b) Time traces of two intensity fluctuations from the raw dataset. The red and blue lines depict the intensity trajectories of two pixels that record the surface temperature above the air structure and the metal substrate, respectively. (c) Degree of the second-order correlation of the intensity fluctuations displayed in (b). Within the correlation time, the measured $g_{\text{Air}}^{(2)}(\tau)$ is larger than $g_{\text{Metal}}^{(2)}(\tau)$, which reveals that the subsurface air structure can be differentiated from the surrounding medium by calculating the second-order correlation.

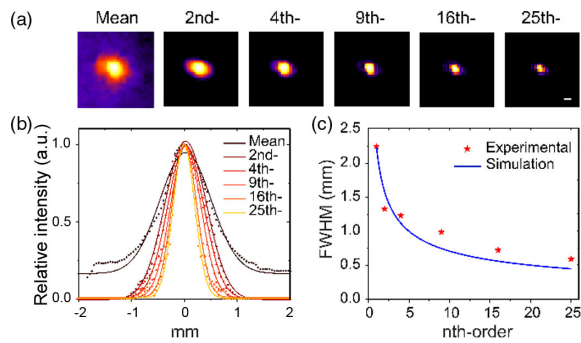


Fig. 3. (a) HG_n images of an isolated thermal emitter. From left to right: mean image (mean intensity of all frames), 2nd-, 4th-, 9th-, 16th-, and 25th-order HG images. Scale bar: 0.5 mm. (b) Gaussian fits of the cross section of the thermal emitter displayed in (a). Dots, experimental data; solid curves, Gaussian fit. (c) Comparison of experimental and simulated resolution enhancement. Red stars, FWHM of the fits displayed in (b); blue curve, \sqrt{n} -fold resolution improvement of HG_n images.

cannot figure out what the structure is beneath the coating tape. Figure 4(b) displays the mean image and the 2nd-, 4th-, 9th-, 16th-, and 25th-order correlation images of the thermal target of the sample. Since the maximum distance $r_5 = 1.2$ mm between two close-by targets beneath the surface tape layer is smaller than the resolution limit $D_0 \approx 2.21$ mm, the subsurface air grooves cannot be differentiated from each other in the original mean image. By employing the calculation of the high-order correlations, as is shown in Fig. 4(b), the air grooves are clearly revealed with improved resolution. In addition, the image quality, especially the contrast and the resolution, has been dramatically enhanced in the HG_n images.

In conclusion, we have theoretically and experimentally demonstrated the resolution enhanced subsurface PTI by using the high-order correlation imaging method. We have quantified the resolution limit of the obtained far-field IR thermal images with the thermal point spread function and HWHC of the amplitude contrast function. Later, we showed that the width of an isolated thermal emitter can be reduced by calculating the high-order correlations, which indicates that the method works well for enhancing resolution in PTI. Finally, we have applied this method for imaging a subsurface air structure in an opaque sample. For future work, we can improve the temporal resolution limitation during image acquisition by increasing the

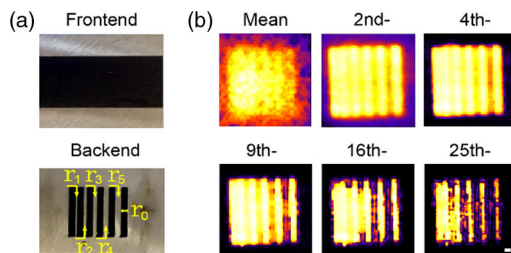


Fig. 4. Application of HG imaging method in PTI. (a) Six air grooves with each groove width of $r_0 = 1$ mm are dug on the metal substrate of the opaque double-layer sample. The pitches of the grooves are $r_1 = 0.4$ mm, $r_2 = 0.6$ mm, $r_3 = 0.8$ mm, $r_4 = 1$ mm, and $r_5 = 1.2$ mm. (b) The mean image and the resolution enhanced HG_n images by using 2nd-, 4th-, 9th-, 16th-, and 25th-order correlations. Scale bar: 1 mm.

modulation rate to 10 Hz, and, with an IR camera with a quicker sampling rate (e.g., 60 Hz) with a proper correlation order, the expected time consumption can be reduced more than 40 times. This method is expected to be helpful for industrial applications such as measuring the porosity of ceramic coatings [26] and inspection of aircraft structural components [27]. Besides, it is appealing in the medical diagnostic inspection of biological tissues/turbid media (e.g., dental samples) [28]. This technique enables a new route for high-resolution subsurface imaging in biomedical applications and optical metrology.

Funding. National Natural Science Foundation of China (11304201, 11674228, 61475100); National Key Research and Development Program of China (2016YFA0302500).

Disclosures. The authors declare no conflicts of interest.

REFERENCES

- G. C. Wetsel and F. A. McDonald, *Appl. Phys. Lett.* **41**, 926 (1982).
- L. J. Inglehart, K. R. Grice, L. D. Favro, P. K. Kuo, and R. L. Thomas, *Appl. Phys. Lett.* **43**, 446 (1983).
- F. A. McDonald, G. C. Wetsel, and S. A. Stotts, *Acoustical Imaging* (Springer, 1982).
- K. H. Choi, J. Meijer, T. Masuzawa, and D. H. Kim, *J. Mater. Process. Technol.* **149**, 561 (2004).
- B. Bertussi, J.-Y. Natoli, and M. Commandré, *Appl. Opt.* **45**, 1410 (2006).
- P. D. Samolis and M. Y. Sander, *Opt. Express* **27**, 2643 (2019).
- J. C. Murphy and L. C. Aamodt, *Appl. Phys. Lett.* **38**, 196 (1981).
- H. A. Willis, S. J. Sheard, and M. G. Somekh, *Proc. SPIE* **0917**, 78 (1988).
- K. Friedrich, K. Haupt, U. Seidel, and H. G. Walther, *J. Appl. Phys.* **72**, 3759 (1992).
- G. C. Wetsel and F. A. McDonald, *J. Appl. Phys.* **56**, 3081 (1984).
- K. R. Grice, L. J. Inglehart, and R. L. Thomas, *J. Appl. Phys.* **54**, 6245 (1983).
- S. B. Ippolito, S. A. Thorne, and B. B. Goldberg, *Appl. Phys. Lett.* **84**, 4529 (2004).
- J. Miyazaki, H. Tsurui, and T. Kobayashi, *Opt. Express* **22**, 18833 (2014).
- J. Miyazaki and T. Kobayashi, *Biomed. Opt. Express* **6**, 3217 (2015).
- J. Miyazaki, H. Tsurui, and T. Kobayashi, *Opt. Express* **23**, 3647 (2015).
- T. Dertinger, R. Colyer, G. Iyer, S. Weiss, and J. Enderlein, *Proc. Natl. Acad. Sci. USA* **106**, 22287 (2009).
- S. W. Hell and J. Wichmann, *Opt. Lett.* **19**, 780 (1994).
- M. G. L. Gustafsson, *Proc. Natl. Acad. Sci. USA* **102**, 13081 (2005).
- S. T. Hess, T. P. K. Girirajan, and M. D. Mason, *Biophys. J.* **91**, 4258 (2006).
- M. J. Rust, M. Bates, and X. Zhuang, *Nat. Methods* **3**, 793 (2006).
- M. Kim, C. Park, C. Rodriguez, Y. Park, and Y. H. Cho, *Sci. Rep.* **5**, 16525 (2015).
- T. Dertinger, R. Colyer, R. Vogel, J. Enderlein, and S. Weiss, *Opt. Express* **18**, 18875 (2010).
- S. C. Stein, A. Huss, D. Hähnel, I. Gregor, and J. Enderlein, *Opt. Express* **23**, 16154 (2015).
- Y. Liu, L. Chen, W. Liu, X. Liang, and W. Wan, *Appl. Opt.* **58**, 2350 (2019).
- Y. Zhou, J. Liu, J. Simon, and Y. Shih, *J. Opt. Soc. Am. B* **29**, 377 (2012).
- C. Meola, G. M. Carlomagno, A. Squillace, and G. Giorleo, *Meas. Sci. Technol.* **13**, 1583 (2002).
- D. Wu, J. Rantala, W. Karpen, G. Zenzinger, B. Schönbach, W. Rippel, R. Steegmüller, L. Diener, and G. Busse, *Review of Progress in Quantitative Nondestructive Evaluation* (Springer, 1996), pp. 511–518.
- N. Tabatabaei, "Development of frequency and phase modulated thermal-wave methodologies for materials non-destructive evaluation and thermophotonic imaging of turbid media," Ph.D. thesis (Department of Mechanical and Industrial Engineering, University of Toronto, 2012).